Proceedings of the ASME 2017 Pressure Vessels and Piping Conference
SAND2017-3432C
PVP2017
July 16-20, 2017, Waikoloa, Hawaii, United States

PVP2017-65118

A CASE STUDY FOR THE LOW FIDELITY MODELING OF THREADED FASTENERS SUBJECT TO TENSILE LOADINGS AT LOW AND HIGH STRAIN RATES

John P. Mersch
Sandia National Laboratories
Albuquerque, NM, United States

Jeffrey A. Smith
Sandia National Laboratories
Albuquerque, NM, United States

Evan P. Johnson
Sandia National Laboratories
Albuquerque, NM, United States

ABSTRACT

A series of tests on NAS1352-06-6P threaded fasteners were coupled with analysis to fit constitutive models, evaluate multiple modeling approaches, and ultimately predict failure. Experiments loading the fasteners in tension at both quasistatic and dynamic loading rates were performed to obtain calibration and validation data for the analysis. The fastener was modeled with two low-fidelity approaches – a "plug" of hex elements retaining the nominal fastener geometry (without threads) and a "spot weld", which incorporates similar geometry but the fastener is sliced near its mid-plane to define a tensile load-displacement relationship between the two exposed surfaces – to accommodate the use of these modeling methods in a larger, more detailed finite element analysis. Both modeling approaches were calibrated using quasistatic test data and then extended to the dynamic analyses to compare with the analogous test results. The analysis accurately reproduces most acceleration time-histories observed in the dynamic testing but under predicts failure, indicating the possible presence of strain rate effects that have been neglected in the constitutive models.

INTRODUCTION

Researchers have been utilizing finite element analysis for many years to investigate the behavior of fasteners and bolted joints. Some of the early research in this area was conducted by Krishnamurthy and Graddy, who led a program in the 1970s to investigate the behavior of end plate connections through 2D and 3D finite element analysis and testing [1]. Around the same time, Maruyama used an axisymmetric model with threads to analyze the stresses in a bolt-nut joint [2]. A few years later, Bretl and Cook also used an axisymmetric model and attempted to mimic the thread zone by placing a layer of elements with orthotropic properties around the outside of the bolt to evaluate stresses in the mating materials [3].

As computational capacity has continued to grow, increasingly detailed three-dimensional fastener models that include threads and capture their interactions with mating materials have been developed and analyzed [4-8]. Castelluccio and Brake recently illustrated this capability with multiple models of varying fidelities to identify important fastener model characteristics and quantify their uncertainties [9]. Franplass, Langseth, and Hopperstad created models with similar fidelity and extended their study to tensile loadings at high strain rates utilizing a split Hopkinson bar for testing, where they found a significant strain rate dependence in M5 threaded rods made of carbon steel in property class 4.6 [10,11]. High fidelity fastener models have been thoroughly exercised and continue to grow into increasingly complex studies.

While this detailed modeling captures the complex behavior of the threads and mating body interactions, this level of fidelity cannot be incorporated in analyses where fasteners are part of a much larger, more detailed model. It thus becomes necessary to model fasteners with a lower level of fidelity yet still capture the global behavior of the joint, especially when its performance is critical to the output quantities of interest. A variety of low fidelity approaches have been incorporated across a broad spectrum of applications in an effort to capture relevant behavior at low computational cost. One approach to bolt and fastener modeling has been to create a "plug" of material that includes the bolt head and shank, but no explicit modeling of the connection or threads. Bursi and Jaspart tested and analyzed tee-stub connections, benchmarking the performance of their FE model that included a plug-like representation of the bolt [12]. Ju, Fan, and Wu modeled the fastener in a similar way while studying the behavior of the butt-type steel bolted joint [13]. Fernandez, Pernia, Martinez-de-Pison, and Lostado also utilized a plug-like approach, and combined their FE model with data mining and artificial intelligence to predict behavior in other tests [14].

Other simple methods have been used to simulate fastened joint behavior in analysis. Knight Jr., Phillips, and Raju did not explicitly model the bolt, washer, and nut in their configuration, but represented the bolt with 1-D linear elastic beam elements and used kinematic coupling constraints to simulate the effects of the washer [15]. Razavi, Abolmaali, and Ghassemieh used an elastic "invisible bolt" to simplify their finite element analysis

while still modeling the behavior of the bolted connection [16]. Many modeling approaches have been incorporated in finite element analyses to solve a diverse set of fastener problems, but no literature was found that compared and contrasted the implementations of these approaches and attempted to assess which methods perform best.

Further bolt modeling complications arise from the challenges associated with acquiring applicable test data for calibration and validation. Performing high strain rate tests can be difficult and may place unacceptable constraints on the time and budget of a project. Even the quasistatic testing of fasteners is nontrivial as local displacement measurements typically cannot be obtained and must be replaced by global measurements that include the compliance of all bodies associated with the test (test fixtures, bushings, washers, etc.). Failure to account for all deformation contributing to the displacement measurements can lead to misinformed material properties that poorly reproduce the behavior seen in these basic tests and therefore cannot be reliably extended to other applications.

The work summarized below details a case study where two low fidelity modeling approaches were investigated to better understand proper calibration and ultimately assess their performance when subjected to multiple loading rates. Experiments loading NAS1352-06-6P threaded fasteners in tension at both quasistatic and dynamic loading rates were performed to guide material modeling and evaluate the performance of two modeling approaches – a "plug" of hex elements retaining the nominal fastener geometry (without threads) and a "spot weld", which incorporates similar geometry but the fastener is sliced near its mid-plane in order to define a tensile load-displacement relationship between the two exposed surfaces. Both approaches were calibrated to quasistatic test data and then incorporated in the dynamic analyses to assess their performance when extended to high strain rate applications.

NOMENCLATURE

DVRT	Differential Variable Reluctance Transducer
eqps	equivalent plastic strain
MLEP	multi-linear elastic-plastic
Sierra/SM	Sierra Solid Mechanics

TEST DESCRIPTIONS

Two unique test fixtures were designed and built to test the fasteners at quasistatic and dynamic loading rates in tension. Both tests are briefly described in the following sections. Dimensions of the NAS1352-06-6P fasteners were measured prior to quasistatic testing and are provided in Table 1. For additional fastener details and dimensions, refer to the NAS1352 datasheet [17].

Quasistatic

The quasistatic test apparatus shown in Fig. 1 is composed of the 4340 steel test fixtures, 4340 steel bushings, and steel fastener (Fig. 2). Displacement data for each test was collected by four DVRTs (Fig. 3) located 0.75 in (19.1 mm) from the axis of the fixture which measure the gap between the top and bottom bushings. Tests were performed on both preloaded fasteners torqued to 20 in-lb (2.26 N-m) and non-preloaded fasteners (hand tightened).

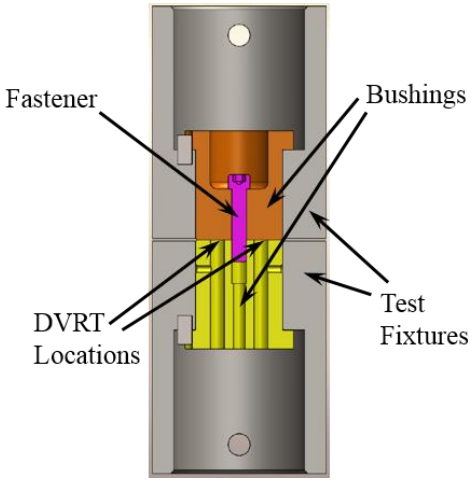

Figure 1: Quasistatic Tension Test Setup


Figure 2: NAS1352-06-6P Fastener


Figure 3: DVRT Locations

Dynamic

The dynamic tension test apparatus is shown in Fig. 4 and includes the Al6061-T6 fixture base, SS304L fixture lid, A36 steel 1.0 lb (0.454 kg) tensile mass, 4340 hardened steel bushing, and steel fastener. To create a dynamic loading scenario the test fixtures were bolted to the carriage of a bungee accelerated drop table (see Fig. 5). When the drop table carriage impacts the reaction mass the fastener experiences a tensile loading caused by the acceleration of the tensile mass. Depending on the impact magnitude the screw is unchanged, loses preload, or fails catastrophically, where a catastrophic failure was defined as the screw being pulled into two separate pieces.

Table 1: Dimensions of Quasistatic Tension Specimens and Analysis Model

NAS1352-06-6P	Specimen 1	Specimen 2	Specimen 3	Specimen 4	Specimen 5	Specimen 6	Specimen 7	Model
Head Diameter, A (in)	0.222	0.223	0.222	0.224	0.224	0.221	0.224	0.226
Head Height, H, (in)	0.1367	0.1365	0.1372	0.1372	0.1371	0.1372	0.1369	0.138
Shank Length, L, (in)	0.3688	0.364	0.3673	-	0.3639	0.3618	0.3686	0.375
Major Diameter, D, (in)	0.134	0.133	0.134	0.134	0.135	0.134	0.135	N/A
Tensile Stress Area, A_S, (in^2)	0.0084	0.0083	0.0084	0.0084	0.0086	0.0084	0.0086	0.0084

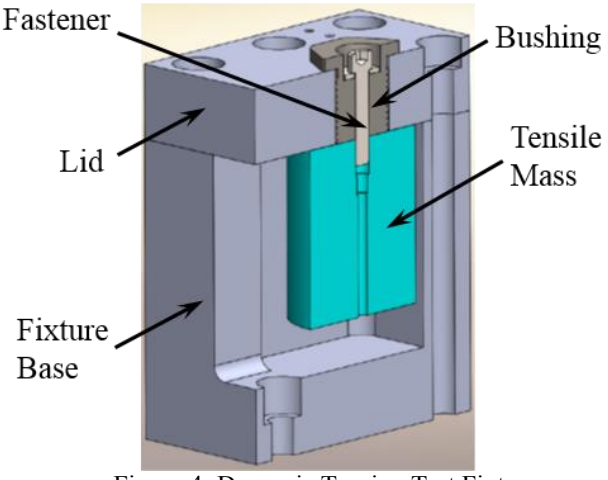

Figure 4: Dynamic Tension Test Fixture

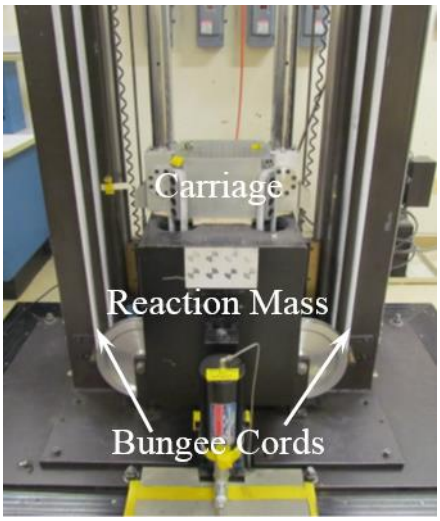

Figure 5: Dynamic Testing Experimental Setup

Endevco model 7270 and 7274 piezoresistive accelerometers were used to measure the acceleration on the carriage, test fixture, and mass. All tests were performed with the fasteners preloaded to 22 in-lb (2.49 N-m). The main objective was to determine the force at which the screw under test catastrophically fails while varying the shape of the pulse acceleration. Five pulse levels were chosen that spanned the entire range of the drop table capability. Four fasteners were tested at each velocity level with the intent of bracketing the failure point within those four tests. With only four screws to test at each velocity level it was critical to bracket the failure point by achieving both a catastrophic failure and a non-failure within the four tests. This methodology worked well as there were no instances that yielded inconclusive data throughout the entire test series. Some test levels, however, yielded a higher resolution on the failure point than others.

ANALYSIS MODELS

Fastener Modeling

The fastener is modeled with two different approaches. The first, a plug of hex elements, incorporates the fastener head and shank (without threads) and models the threaded connection with tied contact. An elastic-plastic constitutive model is used for all fastener elements where the piecewise linear hardening curve is calibrated using one of the experimental quasistatic data sets. A death criterion was defined to model failure by approximating the maximum equivalent plastic strain (eqps) that reproduces the displacement-to-failure observed in testing. The fastener was meshed with approximately 0.0065 inch elements in order to have 16 elements through the diameter. The plug mesh is shown in Fig. 6 (left) where it is colored by an equivalent plastic strain contour (scale also shown in Fig. 6).

The second modeling approach, the spot weld, incorporates similar geometry and mesh but the fastener is sliced near its mid-plane in order to define a tensile load-displacement relationship between the two exposed surfaces. While the fastener is still explicitly modeled, it is given elastic properties to minimize its displacement and allow the spot weld to govern the fastener behavior. This modeling approach is calibrated to the same quasistatic data set as the plug, and tied contact is again used to join the relevant fastener nodes to the mating body. The spot weld implementation is illustrated in Fig. 6 (right). The gap seen in the fastener is where the spot weld is defined – a load-displacement relationship governs the behavior between the two fastener surfaces.

Dimensions of the fastener in the analysis model are provided in Table 1. Note that the cross-sectional area of the analysis model fastener was set equal to the average of the tensile stress areas measured from the seven specimens. Since there are no threads in the model, the major diameter is not provided.

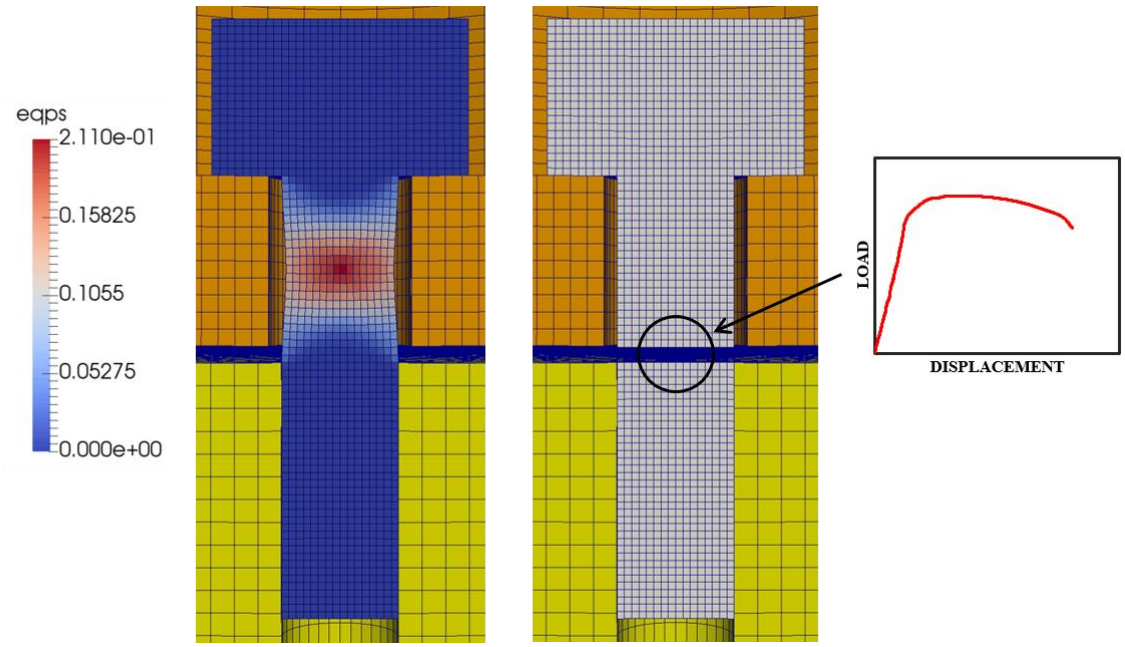

Figure 6: Plug (Left) and Spot Weld (Right) Implementations (Shown in Dynamic Analysis Model)

Quasistatic Analysis

One-quarter of the quasistatic setup is modeled utilizing symmetry of the design and is shown in Fig. 7. The fixtures and bushings are modeled as elastic bodies with representative 4340 steel properties. A prescribed displacement is applied to the top of the test fixture, and a nodeset is created at the DVRT locations to enable direct comparisons to the test results. Simulations are performed using the code Sierra/SM and 8-node**,** uniform gradient hex elements are used for all geometry. Material properties for the fastener and 4340 steel are provided in Table 2.

It should be noted that the quasistatic plug approach simulations were performed with the implicit module of Sierra/SM, but the spot weld simulations were performed in the explicit module because the implementation is not available for implicit analyses in Sierra/SM. These spot weld simulations are performed over small time durations (32 ms) as conducting these analyses at quasistatic loading rates would be infeasible.

Dynamic Analysis

One-half model symmetry is utilized for the dynamic testing setup which is also shown in Fig. 7. The 4340 steel blocks are modeled with the Johnson-Cook constitutive model, the Al6061 and SS304L blocks are modeled using an elastic-plastic model with piecewise-linear hardening, and the A36 is modeled with power-law hardening. Material properties for the dynamic simulations are provided in Table 3. Simulations are performed using the explicit module of the code Sierra/SM and 8-node**,** uniform gradient hex elements are used for all geometry.

The drop table tests are simulated by prescribing a pulse acceleration to reproduce the test loading. The pulse takes the form of,

$$K \sin^2\left(\frac{\pi t}{\tau}\right) \quad (1)$$

where K is the pulse amplitude in in/s^2, t is the time after impact, and τ is the baseline pulse duration in seconds. An example of a test pulse and the analysis approximation is shown in Fig. 8. In some cases, the beginning and end of the test pulse was ambiguous (as illustrated in Fig. 8), and the duration of the analysis pulse was fit to best represent the data. This prescribed acceleration is analytically applied to the bottom of the test fixture where it attaches to the drop table carriage during testing.

Table 2: Quasistatic Analysis Material Properties

Quasistatic Material Properties	St4340	Fastener
Density, ρ (snails/in^3)	0.0007133	0.000725
Young's Modulus, E (psi)	3.04E+07	2.85E+07
Poisson's Ratio, ν	0.3	0.33
Yield Stress, σ_y (psi)	73000	153000

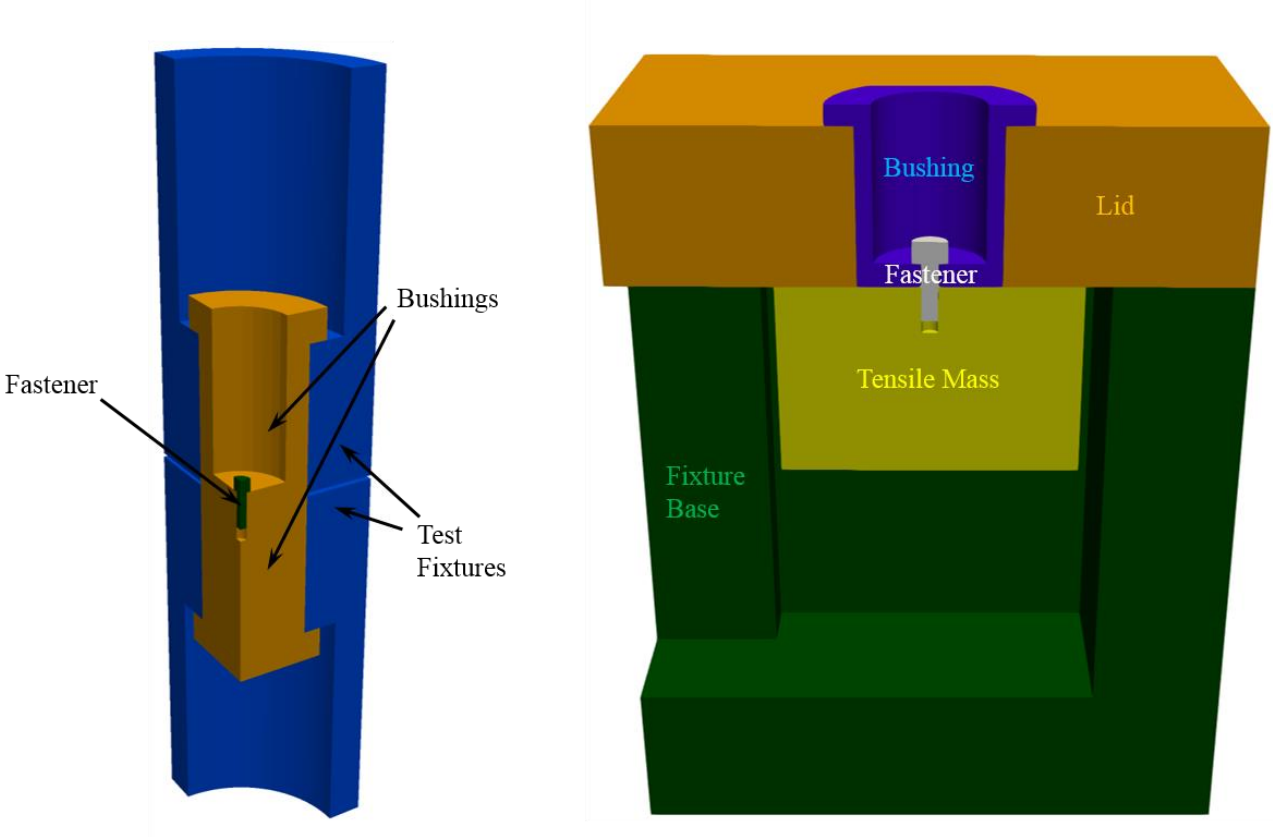

Figure 7: Quasistatic (Left) and Dynamic (Right) Analysis Models

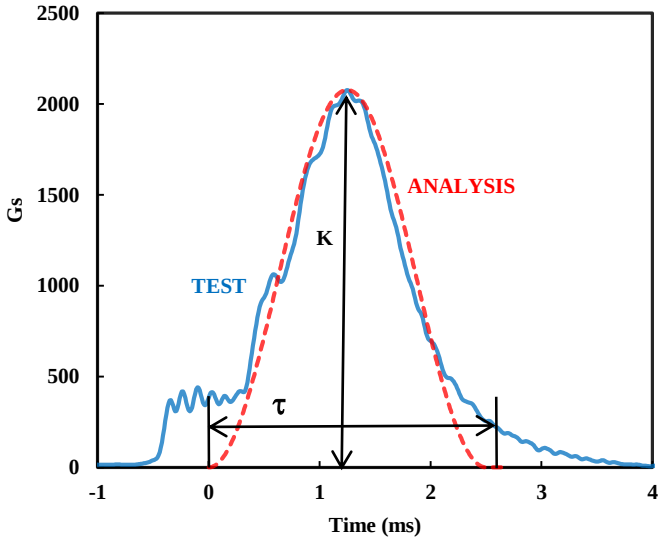

Figure 8: Example of Pulse Acceleration

Table 3: Dynamic Analysis Material Properties

Dynamic Material Properties		Al6061	SS304L	St4340	A36	Fastener
Basic	Density, ρ (snails/in^3)	0.000254	0.000732	0.000713	0.000724	0.000725
	Young's Modulus, E (psi)	1.00E+07	2.80E+07	3.04E+07	3.00E+07	2.85E+07
	Poisson's Ratio, ν	0.3	0.3	0.3	0.3	0.33
	Yield Stress, σ_y (psi)	45000	36200	249000	37400	150000
MLEP	Beta	1	1	-	-	1
	Critical Tearing Parameter, t_p	1.586	12.04	-	-	-
	Critical Crack Opening Strain	0.1	0.1	-	-	-
Johnson-Cook	Hardening Constant, B (psi)	-	-	157800	-	-
	Hardening Exponent, n	-	-	0.26	-	-
	Density*Specific Heat, ρC_v (lb/in^2.K)	-	-	298	-	-
	Rate Constant (C)	-	-	0.014	-	-
	Thermal Exponent (m)	-	-	1.03	-	-
	Reference Temperature (T_{ref})	-	-	298	-	-
	Melting Temperature (T_{melt})	-	-	2768	-	-
Powerlaw Hardening	Hardening Constant, A (psi)	-	-	-	700000	-
	Hardening Exponent, m	-	-	-	0.38	-
	Luders strain	-	-	-	0.0057	-

TEST AND ANALYSIS RESULTS

Plug Calibration

The plug approach was calibrated using load-displacement data from the quasistatic test series to fit the piecewise-linear hardening curve; however, this process was complicated by the significant difference in the displacement data obtained from the stroke and DVRT measurements. A plot comparing these measurements is shown in Fig. 9. The linear elastic regions of these curves have dramatically different slopes and the stroke measurement is 25% larger than the DVRT at failure. These results suggest that compliance from test fixtures, bushings, and the test machine significantly contributed to the data, thus requiring the analysis to not only accurately model the fastener and its behavior, but all bodies contributing to the respective measurement. These differences have important consequences on the fitting process – if the calibration model cannot separate the deformation of the fastener from the deformation of test fixturing, then this model cannot be reliably extended to other applications. Thus, the DVRT measurement was used to evaluate the constitutive model calibration as it is a more local measurement than the stroke and likely provides a more reliable validation source.

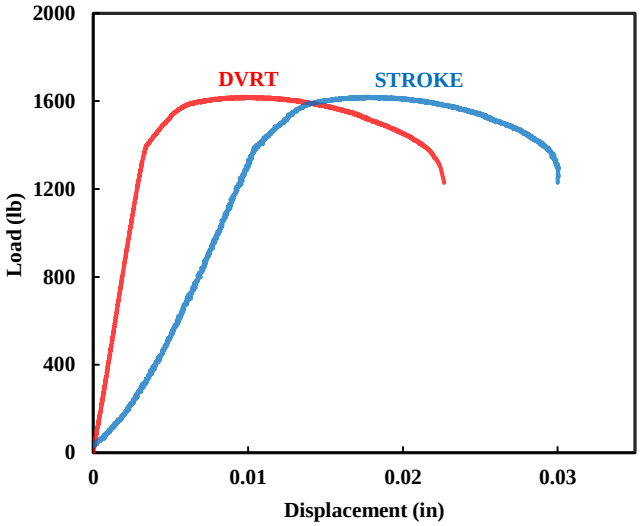

Figure 9: Load-Displacement Responses from Tension Test

The load-displacement curve from the calibrated plug approach is compared to test data in Fig. 10. A non-preloaded test from the quasistatic test series was used to perform the fit. Only the hardening curve of the constitutive model was calibrated while the elastic properties of each material in the analysis were preserved, creating the difference in the linear-elastic regions seen in the figure.

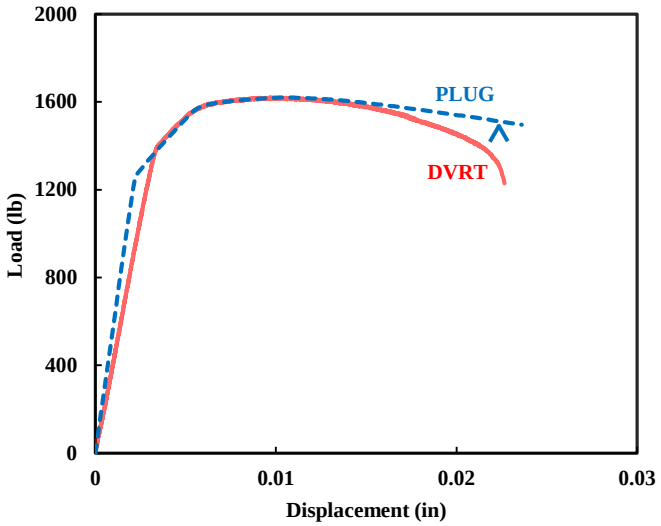

Figure 10: Plug Analysis Calibration Results – Load-Displacement Response

The analysis reasonably reproduces the test results, but does not completely capture the load reduction seen post peak stress. The triangular mark seen in the figure denotes the point at which the eqps failure criterion (eqps=0.211) fails the fastener, which corresponds to a displacement of approximately 0.212 in (5.38 mm). This is a slightly conservative approximation, as the test fails at a displacement of 0.226 in (5.74 mm). This failure criterion is carried throughout the rest of the analysis and used to evaluate the dynamic simulations against test results.

Spot Weld Calibration

The spot weld was also fit with the same data set, and the input and output load-displacement curves from the calibrated model are shown in Fig. 11 and compared to test data.

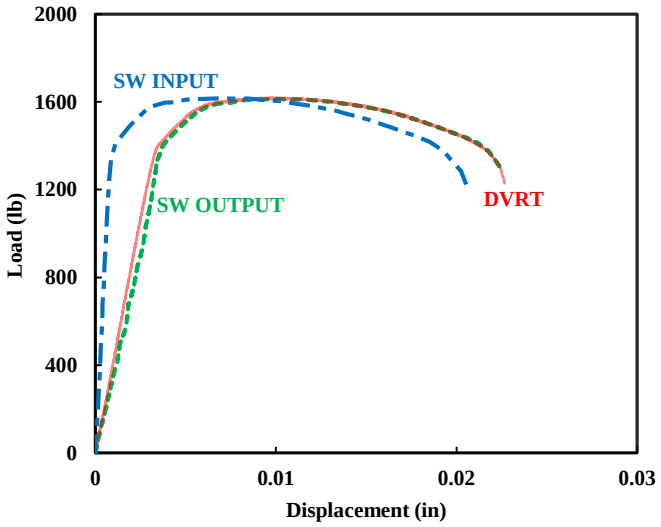

Figure 11: Spot Weld Calibration Results – Load-Displacement Response

The effect of bushing and test fixture compliance is reiterated in these results, as the load-displacement input that governs the behavior between the two fastener faces is appreciably different than the output load-displacement response gathered at the DVRT location. However, once this compliance is considered, the spot weld very accurately reproduces the load-displacement curve and better captures the response post peak load.

Dynamic Tension Results

The constitutive models presented in the previous sections were next incorporated in the dynamic analyses to assess their performance at high strain rates. Simulations using both modeling approaches were run at fixed acceleration pulse durations while increasing the peak acceleration by 25 G increments until failure occurred. The simulation results for the plug and spot weld are compared to test data in Fig. 12, where the peak acceleration of the pulse in Gs is displayed on the y-axis and the width of the pulse in ms is displayed on the x-axis. There are two test curves shown in the figure, where the space below the bottom curve represents loading scenarios that will not cause the screw under test to fail catastrophically, and the space above the top curve represents loading scenarios that will cause the screw under test to fail catastrophically. The space between the test curves represents the loading gap between a test that failed the fastener and a test where the fastener remained intact.

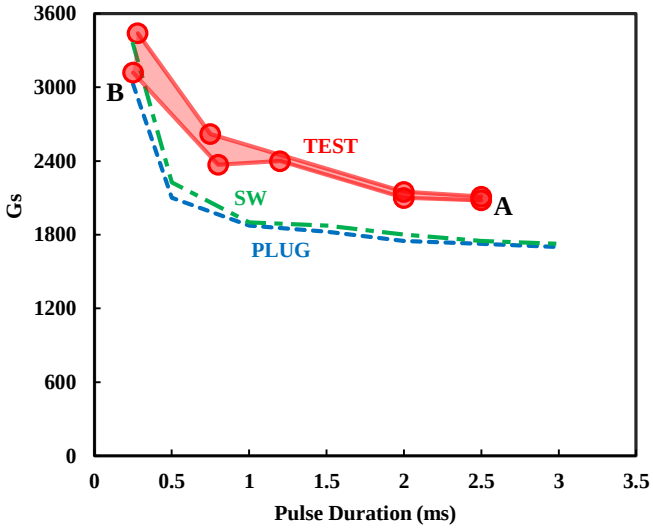

Figure 12: Test-Analysis Comparison – Dynamic Tension Failure Curves

The failure curves of both modeling approaches are similar and differ by less than 100 Gs for most pulse durations. At small pulse durations the spot weld carries slightly more load, but beyond 0.5 ms the loads are essentially identical. Both modeling approaches reproduce the test data response shape, but overall the analysis load magnitudes are consistently 300-500 Gs less than the test data. While this is a conservative failure estimate, these magnitudes represent ~20-25% error.

The gap observed between the test and analysis failure curves led to a study of the acceleration data collected throughout the testing series to further assess the reliability of the simulations. Simulations were performed at the test conditions for test case A (pulse duration = 2.5 ms, denoted in Fig. 12 with an "A") and test case B (pulse duration = 0.297 ms, denoted in Fig. 12 with a "B") and accelerations were analytically monitored for the carriage, test fixture, and mass to compare to the test measurements. The test accelerations from case A are shown in Fig. 13, a comparison of test and analysis results for case A is shown in Fig. 14, and a comparison of test and analysis results for case B is shown in Fig. 15, where test results are plotted with solid lines and analysis results with dashed lines. Note the fixture accelerations are excluded from Fig. 14 because they are essentially identical to their carriage counterparts.

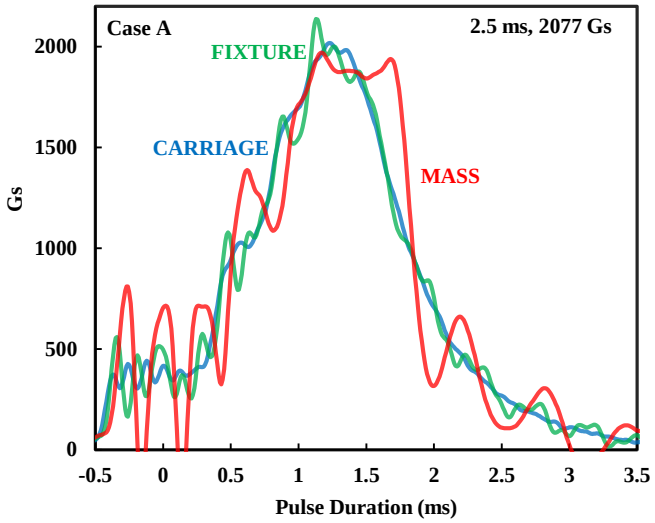

Figure 13: Experimental Accelerations for Test Case A

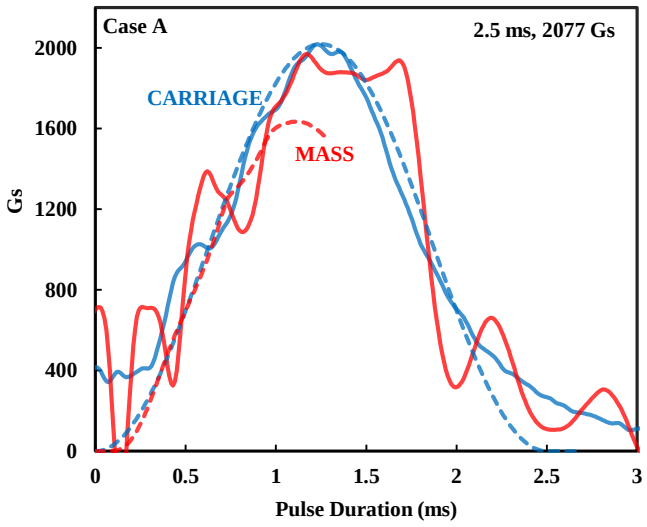

Figure 14: Test-Analysis Comparison for Case A – Accelerations (Solid Lines for Test, Dashed for Analysis)

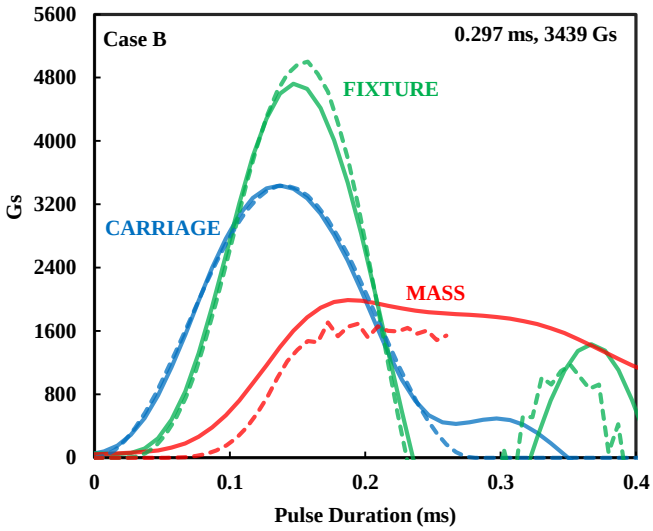

Figure 15: Test-Analysis Comparison for Case B – Accelerations (Solid Lines for Test, Dashed for Analysis)

The accelerations of the carriage, fixture, and mass obtained from testing have similar shapes and peak accelerations for case A (Fig. 13) where the pulse duration was the largest of the dynamic test series. However, as the pulse duration gets smaller, the peak accelerations of the carriage, fixture, and mass begin to deviate as seen in the results for test case B (Fig. 15), where the pulse duration was the smallest of the test series. An observation of note is that the peak acceleration of the mass is nearly constant between the two loading conditions, as it is 1950 Gs and 1992 Gs in test cases A and B, respectively.

Although there are slight differences, the prescribed acceleration in the analysis (analysis carriage acceleration) seems to approximately reproduce the carriage test acceleration time-history, and the time-histories of the test fixture also compare favorably. The main difference in the test and analysis results seems to be between the peak accelerations of the mass, where the test data is typically in the range of 1920-2000 Gs while the analysis is in the range of 1630-1710 Gs. This discrepancy is similar to the gap between the end of the failure curves in Fig. 12 where the tests and analysis predict failure for a 2.5 ms pulse at 2077 Gs and 1725 Gs, respectively.

This observation make sense upon further consideration for the analysis – a simple free body diagram indicates that the acceleration of the mass is equivalent to the load carried by the fastener, and intuitively the failure curve in Fig. 12 should trend toward the load carrying capacity of the fastener observed in quasistatic testing (approximately 1620 lb). Extending this logic to the test data leads to a more interesting conclusion; the tensile mass peak accelerations (Fig. 14 and Fig. 15) are significantly higher than the quasistatic ultimate load of the fastener (approximately 20%), indicating the fastener is carrying more load at increased strain rates which the current strain rate independent constitutive model cannot capture.

DISCUSSION AND CONCLUSIONS

Fasteners present unique modeling challenges due to their intricate geometry and the difficulty associated with gathering pertinent test data for constitutive model calibration. Test fixture and bushing compliance (even when made from "strong" materials such as tool steel) can significantly contribute to experimental displacement measurements and must be considered in the calibration process in order to obtain reliable material properties.

The results of this study suggest that the low-fidelity modeling approaches of the plug and spot weld can be reliably used to model fasteners for monotonic quasistatic tensile loadings; however, when the simple constitutive models associated with these approaches are extended to high strain rate applications, they do not capture the apparent strain rate effects observed during testing. Overall, these test results are agreeable with the findings of Franplass et al. [10,11] where they discovered a strain rate dependence on ultimate load for threaded steel rods that is comparable to the magnitudes found in this study. These initial findings warrant an expanded study that includes testing performed at intermediate strain rates (0.1 – 10 ε/s) and a more complex, strain rate dependent constitutive model (i.e. Johnson-Cook) to further assess the performance of these fasteners and obtain a better, more robust analysis model.

ACKNOWLEDGMENTS

The authors would like to gratefully acknowledge the contributions and efforts of Tom Bosiljevic for designing and constructing the quasistatic test setups, performing the quasistatic experiments, and working with the analysis team to create a collaborative environment that facilitated all project efforts.

The noteworthy contributions of Doug Vangoethem are also appreciated, as he helped the authors understand the drop table tests from an analysis perspective and assist in properly modeling the tests.

Sandia National Laboratories is a multi-mission laboratory managed and operated by Sandia Corporation, a wholly owned subsidiary of Lockheed Martin Corporation, for the U.S. Department of Energy's National Nuclear Security Administration under contract DE-AC04-94AL85000.

REFERENCES

1. Krishnamurthy, N., Graddy, D.E., 1976, "CORRELATION BETWEEN 2- AND 3-DIMENSIONAL FINITE ELEMENT ANALYSIS OF STEEL BOLTED END-PLATE CONNECTIONS," Computers & Structures, **6** (4-5), pp. 381-389.
2. Maruyama, K., 1976, "Stress Analysis of a Bolt-Nut Joint by the Finite Element Method and the Copper-Electroplating Method," Bulletin of the Japan Society of Mechanical Engineers, **19** (130), pp. 360-368.
3. Bretl, J.L., Cook, R.D., 1979, "MODELLING THE LOAD TRANSFER IN THREADED CONNECTIONS BY THE FINITE ELEMENT METHOD," International Journal for Numerical Methods in Engineering, **14** (9), pp. 1359-1377.
4. Fukuoka, T., Nomura, M., 2008, "Proposition of Helical Thread Modeling With Accurate Geometry and Finite Element Analysis", Journal of Pressure Vessel Technology, **130** (1), pp. 1-6.
5. Huang, J., Guo, L., 2011, "The Research On the Torque-Tension Relationship for Bolted Joints," Key Engineering Materials, **486**, pp. 242-245.
6. Zhao, L.B., Liu, F.R., Zhang, J.Y., 2010, "3D Numerical Simulation and Fatigue life predition of high strength threaded bolt," Key Engineering Materials, **417-418**, pp. 885-888.
7. Grewal, A.S., Sabbaghian, M., 1997, "Load distribution between threads in threaded connections," Journal of Pressure Vessel Technology, **119** (1), pp. 91-95.
8. Majzoobi, G.H., Sadri, A., Bayat, A., Mahmoudi, A.H., 2007, "A THREE DIMENSIONAL NUMERICAL STUDY OF STRESS DISTRIBUTION IN BOLT-NUT CONNECTIONS", *Proceedings of the 18th IASTED International Conference, Modelling and Simulation,* pp. 452-458.
9. Castelluccio, G.M., Brake, M.R.W., 2016, "On the origin of computational model sensitivity, error, and uncertainty in threaded fasteners," Computers & Structures, Preprint.
10. Franplass, H., Langseth, M., Hopperstad, O.S., 2013, "Numerical study of the tensile behaviour of threaded steel fasteners at elevated rates of strain," International Journal of Impact Engineering, **54**, pp. 19-30.
11. Franplass, H., Langseth, M., Hopperstad, O.S., 2011 "Tensile behaviour of threaded steel fasteners at elevated rates of strain," International Journal of Mechanical Sciences, **53** (11), pp. 946-957.
12. Bursi,O.S., Jaspart, J.P., 1997, "Benchmarks for Finite Element Modelling of Bolted Steel Connections," Journal of Constructional Steel Research, **43** (1-3), pp. 17-42.
13. Ju, S. –H., Fan, C. –Y., Wu, G.H., 2004, "Three-dimensional finite elements of steel bolted connections," Engineering Structures., **26** (3), pp. 403-413.
14. Fernandez, J., Pernia, A., Martinez-de-Pison, F.J., Lostado, R., 2010, "Prediction models for calculating bolted connections using data mining techniques and the finite element method," Engineering Structures., **32** (10), pp. 3018-3027.
15. Knight Jr., N.F., Phillips, D.R., Raju, I.S., 2008, "Simulating the Structural Response of a Preloaded Bolted Joint," AIAA 2008-1842, *49th AIAA/ASME/ASCE/AHS/ASC Structures, Structural Dynamics, and Materials Conference*, AIAA, Schaumburg, IL.
16. Razavi, H., Abolmaali, A., Ghassemieh, M., 2007, "Invisible elastic bolt model concept for finite element analysis of bolted connections," Journal of Constructional Steel Research, **63** (5), pp. 647-657.
17. AIA/NAS – Aerospace Industries Association of America Inc., 2016, "English -- SCREW, CAP, SOCKET HEAD, UNDRILLED AND DRILLED, PLAIN AND SELF-LOCKING, ALLOY STEEL, CORROSION-RESISTANT

STEEL AND HEAT-RESISTANT STEEL, UNRC-3A AND UNRC-2A - Rev 13", AIA/NAS NAS1352.